Optimisation of an air film cooled CFRP panel with an embedded vascular network

M. McElroy[a], A. Lawrie[b], I.P. Bond[c]

[a]*Durability, Damage Tolerance, and Reliability Branch, NASA Langley Research Center, Hampton, VA USA*
[b]*Department of Mechanical Engineering, University of Bristol, Bristol, UK*
[c]*Department of Aerospace Engineering, University of Bristol, Bristol, UK*

Abstract

The increasing use in the aerospace industry of strong, lightweight composite materials in primary structural components promises to substantially reduce aircraft non-pay-load weight, improving fuel consumption and operating profitability. This study explores the extension of composite material to regions of gas turbine engines previously considered too hot for composites with moderate melting points. Throughout the majority of a gas turbine cycle, gas stream temperatures exceed the polymer composite glass transition by a considerable margin. Boundary layer cooling strategies, however, may be adopted in the compression stages to extend the downstream distance that can be constructed using lightweight composites. This paper presents formulation and validation of a numerical model and its use in an optimisation study to develop a systematic process for thermal design of polymer composite structures in 'warm' gas streams. Internal vascular and external boundary layer film cooling strategies are considered.

Keywords: carbon fibre reinforced polymer, film cooling, microvascular, thermal analysis

Pre-publication corresponding author: Mark McElroy mark.w.mcelroy@nasa.gov, +1 757 864 9652, 2 W. Reid St, Mail Stop 188E Hampton, VA 23681

Post-publication corresponding author: Mark McElroy mark.w.mcelroy@nasa.gov, +1 757 864 9652, 2 W. Reid St, Mail Stop 188E Hampton, VA 23681

1. Introduction

The increasing use in the aerospace industry of strong, lightweight composite materials in primary structural components promises to substantially reduce aircraft non-pay-load weight, thereby improving fuel consumption and operating profitability. Use of common polymer based composites for gas turbine engine components, however, can prove challenging due to the fact that the maximum operating temperature for a fibre-reinforced polymer composite is constrained by the glass transition temperature (T_g). Copolla [1] showed that for a composite specimen, mechanical performance degrades rapidly at higher temperatures. In the case of a carbon-fibre reinforced polymer (CFRP), an attractive candidate material for aerospace application, T_g lies in the range 100°C - 200°C [2, 3], with precise values dependent on the details of its composition. Throughout the majority of a gas turbine cycle, gas stream temperatures exceed this range by a considerable margin. Boundary layer film cooling strategies may be adopted, however, in the compression stages to extend the downstream distance that can be constructed using lightweight composites.

From the earliest gas turbine engines of the 1940s, turbine blade weakening at high temperature has been mitigated by passing cool air through hollow cavities within the blades [4], transferring heat away from the metal into the coolant flow. In the 1950s, research was initiated on designs that expel the internal cool air flow into the external hot flow through apertures on the blade surface. This allows coolant to be swept back over the blade, coating the blade surface with a boundary film of cool air [5, 6] that thermally insulates the metal from the hot stream. Film cooling combined with internal heat exchange has been shown to be an effective active cooling approach for turbine blades [7, 8], and modern engine components currently can be designed for gas temperatures downstream of the combustor that exceed the melting point of the metal blades.

While there are a small number of publicly available studies on the use of internal vascular cooling in polymer composite materials, none so far consider the role film cooling can play in improving thermal design. Lyall (2008) examined a stiffened composite panel for satellite electronics systems, containing fluidic microchannels for cooling [9]. This study was developed by Williams (2010) to include structural and thermal analysis [10]. Kozola (2010) explored the use of composite material for a fin with an internal vascular network using water or oil as the coolant. Additionally, a one-dimensional

numerical heat transfer model of the fin surface was developed [11]. Quantifying the overall efficiency of a component containing an internal vascular network is an important question and in their work, Pierce and Phillips (2010, 2011) included a mechanical evaluation of a panel containing vascular cooling networks [12, 13]. Soghrati et al (2013) looked at strategies for woven composites using microchannels [14], and Bejan et al. [15, 16, 17, 18] studied a nature-inspired tree branch geometry.

The aim of this study is to explore the extension of CFRP materials to regions of gas turbine engines previously considered too hot for polymer composites with moderate degradation temperatures. An active cooling strategy consisting of both internal vascular heat exchange and external boundary film cooling is investigated. The vascular network topology in a structural component requires careful consideration to balance thermal efficiency between the vascular and film cooling effects. An optimisation study is performed using a numerical model of a cooled composite panel to better understand this relationship. The optimisation study serves as demonstration of a systematic methodology for thermal design of compressor blades manufactured from polymer composites. Experimental work is included with the purpose of validation of the numerical model. An idealised thin-plate CFRP panel of a thickness, composition, and structural rigidity comparable with low pressure compressor blades is considered.

Sections 2-4 focus on creation of an experimentally-validated, predictive numerical model of thermal behaviour in an actively cooled composite panel. In Section 5, the model is extended for iterative design refinement using an automatic gradient-based optimiser. Proof-of-concept of a thermal design methodology for a vascular/film cooled panel is demonstrated.

2. Thermodynamic modelling

A numerical model was developed to predict the temperature distribution of a thin flat plate subjected to a hot external air flow and actively cooled by an internal vasculature and an external cool film. A compressible finite volume approach is used to simulate the internal vasculatory flow. Fourier's law is solved across the plate to estimate temperature distribution in thermal equilibrium. Film cooling is simulated based on a model derived from the classical solutions for viscous boundary layer growth. The thermal transport from the hot external gas stream towards the plate is estimated from empirical relations governing turbulent entrainment, treating temperature as

a passive scalar. Because compressor blades operate in a strongly adverse pressure gradient, curvature of the blades is limited to ensure flows remain attached. It follows then that blade profiles have a small thickness-to-chord ratio and thus a thin flat plate test model offers a good first approximation to their heat transfer properties. More realistic blade profiles would be a trivial extension to the model.

In this paper, the modelling activity is focused only on non-intersecting vascular topologies to reduce the nonlinearity in the parameter space over which an optimal solution may be found. This restriction is a temporary convenience to ensure conclusions are robust and intuitive, but the proposed methodology is fully generalisable to complex network topologies. Another restriction of the current model is that internal vascular flow remains laminar. Including turbulent flow in this study would introduce highly non-linear heat transfer behavior to the system and thus create a much more challenging optimisation problem. Additionally, while this constraint may normally be satisfied in these cooling flows, a model that accounted for and operated in a regime near turbulent transition could potentially be unduly sensitive to parameter variations that lie within the range of manufacturing tolerances in small cooling ducts. Such sensitivities would curtail the ability, particularly of gradient-based automatic optimisers, to recover robust global performance maxima.

Compressible Euler equations accounting for friction are discretised in one dimension with a first order flux-balance, and the mass flux is adjusted iteratively to satisfy a prescribed downstream exit pressure given imposed upstream pressure and temperature boundary conditions. The following equations are presented with regards to a single control volume, with subscripts 1 and 2 representing the locations at the upstream and downstream faces, respectively. From mass conservation, the outlet velocity is given by

$$v_2 = \frac{\dot{V}_2}{A_{sec}} \tag{1}$$

where A_{sec} is the cross sectional area of the tube. Volumetric flow rate, $\dot{V}_2$, is determined using the ideal gas law and when substituted into (1) yields the form of the mass continuity equation used in the solution given by

$$v_2 = \frac{\dot{m} R_{sp} T_2}{P_2 A_{sec}} \tag{2}$$

where A_{sec} is the cross sectional area of the tube, R_{sp} is the specific gas constant, $\dot{m}$ is the coolant mass flow rate, T is coolant temperature, and P is pressure. Conservation of energy in a steady flow is given by

$$h_1 + \frac{v_1^2}{2} = h_2 + \frac{v_2^2}{2} + Q + W \tag{3}$$

where h is enthalpy, Q is heat, and W is work due to friction (note that h, Q, and W are normalized by mass in this equation). Assuming laminar flow and using a Darcy friction factor, f, the change in pressure as a result of friction, ΔP_f, is given as

$$\Delta P_f \;=\; f\frac{dx}{2r}\frac{\rho v^2}{2} = \frac{64}{Re}\frac{dx}{2r}\frac{\rho v^2}{2} \tag{4}$$

where, dx is the control volume length, r is the control volume radius, v is coolant flow velocity, Re is the Reynolds number, and ρ is coolant density. A low-order approximation is made to the cell centre velocity used for estimating average wall friction, and is set equal to the inlet velocity v_1. Thus (3) can be written as

$$Q = c_p(T_1 - T_2) + \frac{v_1^2 - v_2^2}{2} - A_{wall}\frac{8}{Re}\rho v_1^2 dx \tag{5}$$

where A_{wall} is the surface area of a control volume. The rate of heat transfer, $\dot{Q}$, is obtained after multiplication of (5) by $\dot{m}$.

The heat transfer rate can alternatively be expressed as

$$\dot{Q} = A_{wall}U(T_1 - T_\infty) \tag{6}$$

where T_∞ is external air temperature. Making the same low-order linearisation previously used to derive (5), inlet temperature T_1 is used to represent average temperature over a control volume. Multiplying (5) by $\dot{m}$ and equating with (6) yields a formulation of the energy equation suitable for sequential numerical evaluation of a single vessel from inlet to outlet given as

$$\dot{m}\left[c_p(T_1 - T_2) + \frac{v_1^2 - v_2^2}{2} - A_{wall}\frac{8}{Re}\rho v_1^2 dx\right] = A_e U(T_1 - T_\infty). \tag{7}$$

Equation (7) converges to the exact solution as control volumes tend to zero and boundary conditions are iterated to consistency. The heat transfer

coefficient, U, in (7) was shown by Pierce to vary weakly with mass flux [12]. However, it is shown later in Section 4 where U is treated as a constant, that the model performs well.

Using the form of the continuity equation shown by (2), the initial velocity, v_1, is obtained to use in (7). Conservation of momentum provides a third equation to the system, and is expressed as a Rayleigh condition,

$$P_1 A_{sec} + \dot{m} v_1 = P_2 A_{sec} + \dot{m} v_2 + \Delta P_f A_{sec} \tag{8}$$

The unknown variables T_2, P_2, and v_2 are found by solving (2), (7), and (8) simultaneously for each control volume. Iteration proceeds until boundary conditions are satisfied and mass flux converges.

A two-dimensional numerical evaluation of Fourier's heat conduction law

$$q_{cond} = -kA \left[\frac{dT}{dx} + \frac{dT}{dy} \right] \tag{9}$$

predicts temperature $T(x, y)$ in the thin plate, where variations in the out-of-plane direction are considered negligible. Equation (9) is suitable for isotropic heat flow as the thermal conductivity, k, is the same in the x and y directions. Future versions of the model may be enhanced to be applicable to anisotropic heat flow by designating different heat transfer rates for the x and y directions based on the lay-up of a laminate.

Heat convection from the surrounding air occurring out-of-plane is accounted for using Newton's law of cooling, $q_{conv} = hA(T - T_\infty)$. An implicit second order finite difference scheme is formed from a standard 5-point stencil, in this instance on a regular grid, but the technique is trivially extensible to arbitrary topologies and more generally to three-dimensional models of the blade. Source terms from control volumes and external air temperature are linearly interpolated onto the regular grid. The proposed model of external film cooling from leading-edge apertures uses the well-known Blasius solution [19] to the boundary layer equations, $\delta(x) = 1.72\sqrt{\nu x/u}$, where ν is the kinematic viscosity and u is the free airstream velocity, to estimate the downstream growth of an insulating layer in the direction normal to the plate. A turbulent entrainment hypothesis is used to approximate transverse mixing of coolant air with the hot gas stream at a rate consistent with a spread angle of 12° [20], though in practice such details would be refined by determining values of turbulent intensity from preliminary design simulations. An illustration of modelling assumptions with two internal vascules is

shown in Figure 1. The temperature of the aperture is assumed to be transferred to the insulating film, and the initial film thickness is set to match the aperture diameter.

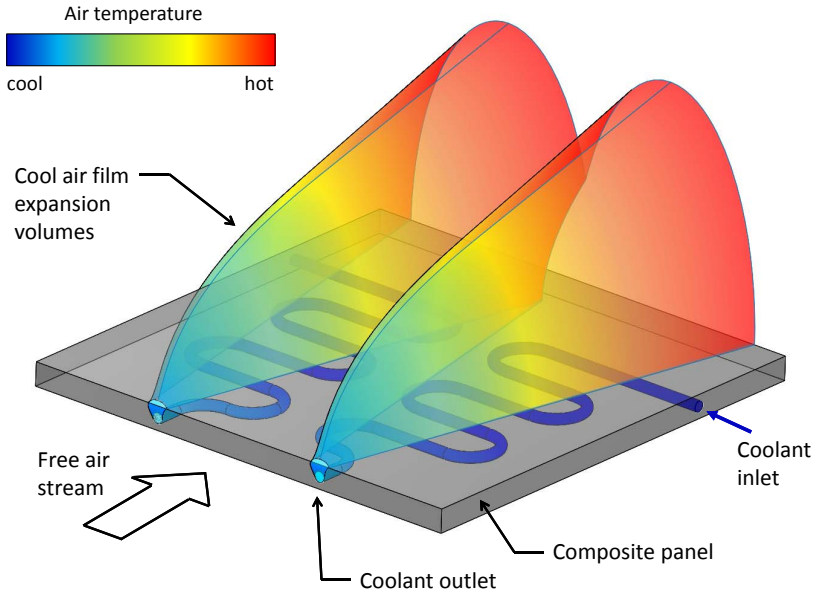

Figure 1: Representative geometry and temperature variation of boundary layer cool air film.

The film air temperature varies along the air stream axis according to

$$T = \left(\frac{A_x - A_o}{A_x}\right) T_\infty + \left(1 - \frac{A_x - A_o}{A_x}\right) T_{exit} \tag{10}$$

where A_o is the initial film section area, A_x is the film section area at a location along the free airstream defined by x, and T_{exit} is the coolant temperature at the aperture. Mixing was assumed to be sufficiently rapid relative to the temperature changes so that the film can be treated as having uniform temperature in a given cross-section.

When the geometry of a cool air film is determined on a panel, the resulting local film temperature replaces the external air temperature source term

T_∞ in (7) in a new solution iteration. The updated T_∞ temperature distribution, in turn, then affects the temperature of the internal vascular coolant flow. Since the internal coolant flow supplies the cool film, an iterative loop is performed until the model solution converges as determined by a change in the standard deviation of the panel temperature from one iteration to the next of less than 1%.

3. Experimental setup

A flat CFRP panel containing a vascular network was fabricated to validate the numerical model described in Section 2. Because the tests are used for model validation purposes, the vascules are placed far apart in order to obtain internal coolant flows uninfluenced by other nearby vascules. Additionally, in this configuration the overlap of contributions on panel temperature reduction from adjacent vascules is minimized. By isolating the flow behavior in each vascule and obtaining an exaggerated panel temperature variance in between vascules, the thermal behavior is somewhat simplified making the tests well suited for model validation.

The vasculature was connected to a compressed air supply and a hot gas stream was passed over the panel. Once in thermal equilibrium, thermal images were taken of the panel using a NEC San-ei Thermotracer Type TH9100MR camera and compared in detail to predictions from the numerical model whose output closely approximates panel surface temperature. The panel was made from carbon/epoxy prepreg manufactured by Gurit and was oven cured as recommended at 70°C for 16 hrs. The lay-up is given by $[\pm 45, 90, 0_3]_s$ and results in a total panel thickness of 2.4 mm. Mechanical performance parameters such as laminate stiffness and strength were not a part of this study. Four centrally located zero degree plies were cut into patterns such that a linear void would exist and define the geometry for a network of four vessels. During lay-up, 1.1 mm diameter Polytetraflouroethylene (PTFE) coated wire was lain along four paths that would form the cooling vessels. During curing, molten resin flows around the PTFE coated wire, and after curing, the wires were pulled out leaving a smooth circular unlined internal void [21]. Fittings were glued to the inlet points of each vessel to connect to an air supply. A photograph and overlaid schematic of the panel and vasculature network geometry is shown in Figure 2.

A hot gas stream from a Bosch heat gun was guided over the panel by a steel diffuser fabricated to match the panel geometry. Pressurized air at

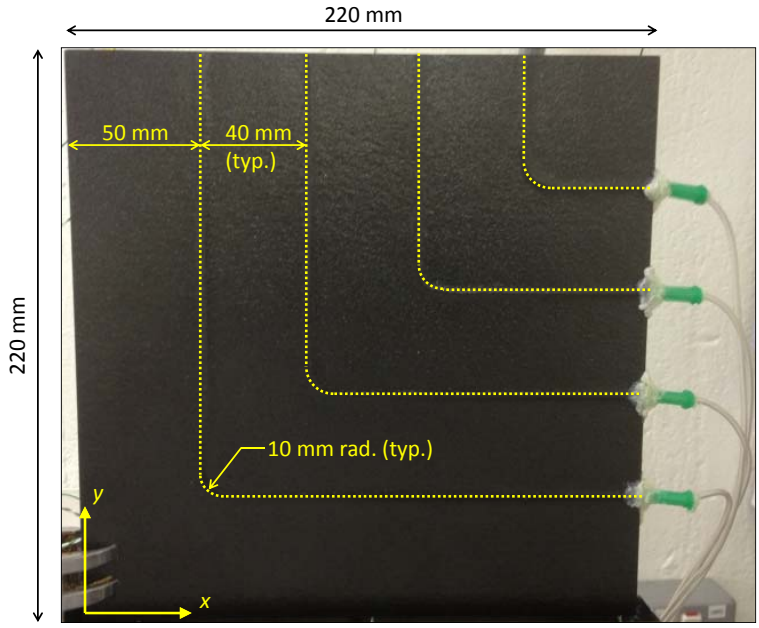

Figure 2: Photograph of composite panel with schematic of embedded cooling vasculature and connected air supply used for numerical model validation.

room temperature was supplied to a reservoir manifold, then distributed to the vessel inlets by pneumatic pipes. The heat gun, diffuser, and panel were assembled in a vertical orientation supported in place by clamps and test stands. A photograph of the experiment is shown in Figure 3. On one side of the panel, six k-type thermocouples were attached to directly measure the air temperature at various locations on the panel and cross-calibrate the thermal imaging camera. Vessel inlet flow temperature was measured using the thermal image of inlet flow pipes just outside the panel. Air flow velocity at the outlet of each vasculature was recorded using an anemometer, which is assumed to be minimally invasive to the flow. At the time of this paper, experimentation that is specifically applicable to the boundary layer film cooling behavior in the model has not yet been performed.

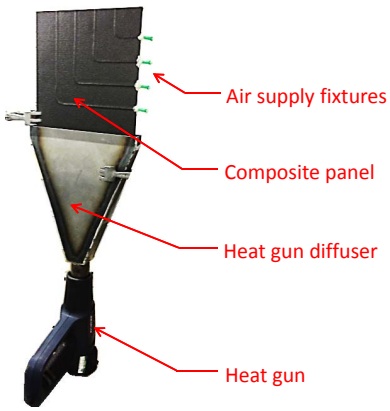

Figure 3: Test apparatus set-up.

4. Model validation

Various external gas stream temperatures were used in testing, but in this paper the focus is only on conditions with a heat gun setting of 140°C. Material properties used in the simulations are shown in Table 1. Figure 4 shows a thermal image of the test panel in thermal equilibrium with no coolant flowing in the internal vessels and as such is representative of the air temperature at the surface of the panel. The panel is hottest at the leading edge and due to the open working section, the external gas stream mixes with the surrounding air and cools exponentially.

To characterize this temperature distribution such that it can be easily used by the numerical model, thermocouple data were gathered at six panel locations and interpolated using an equation of the form, $y = a * exp(b/(x + c))$, in the streamwise direction and linearly in the cross-stream direction. The resulting temperature source distribution used in the thermodynamic model (i.e., T_∞) is shown in Figure 4 and correlates well with the thermal image data of the panel. The correlation in Figure 4 is presented based on the assumption that, at steady state, the panel temperature is the same as the adjacent surrounding air temperature. This assumption appears to be incorrect in the region of the panel less than $y = 0.02$ m. The cause of the difference in panel and adjacent air temperature at this location is unknown, however, it indicates that the air temperature distribution is more complex near the heat gun diffuser outlet than assumed. This slight deficiency in the

Table 1: Material properties used in numerical simulation.

Property	Value	Units	Description
k	1.28	W/mK	conductive heat transfer rate [22]
U	4.0	W/m^{2}K	overall heat transfer coef. (est. [12, 13])
h	9.0	W/m^{2}K	convective heat transfer coefficient [13]
c_p	1005	J/kgK	specific heat of air (20°C)
ν	1.568	(m^2/s) x 10^6	kinematic viscosity of air (20°C)

data correlation method does not affect the validity of using the thermocouple data as a model input for surrounding air temperature.

Using vessel aperture anemometry data and the diameter of the aperture, mass flow rate was estimated for each of the four vessels as

$$\dot{m} = \frac{v_2 P_2 A_{sec}}{R_{sp} T_2} \tag{11}$$

where P_2 is set equal to the ambient room pressure (1 bar). Coolant pressure just upstream of the panel was determined as an input parameter for the thermodynamic model by a calibration process that involved iteratively varying the supply pressure until aperture coolant flow velocity and mass flow rate matched experimental data. Flow velocity and mass flow rate obtained in one test are shown in Figure 5 and correlate well with values obtained from the numerical model using a calibrated air supply pressure of 1.2 bar. Each pair of data points along the horizontal axis corresponds to one vessel in the panel shown in Figure 2.

Figures 6 and 7 show a strong correlation between experiment and numerical predictions over a moderate range of coolant mass fluxes using a heat gun setting of 140°C. In addition to the visual temperature contour images, temperature profiles at cross-sections X-X and Y-Y are shown covering in detail the vessel inlet and outlet regions of the panel. Also, based on this match, one can conclude that the test panel lay-up defined in Section 3 results in approximately isotropic heat flow and hence the use of equation (9) is appropriate for modelling this specimen. The model's good correlation with

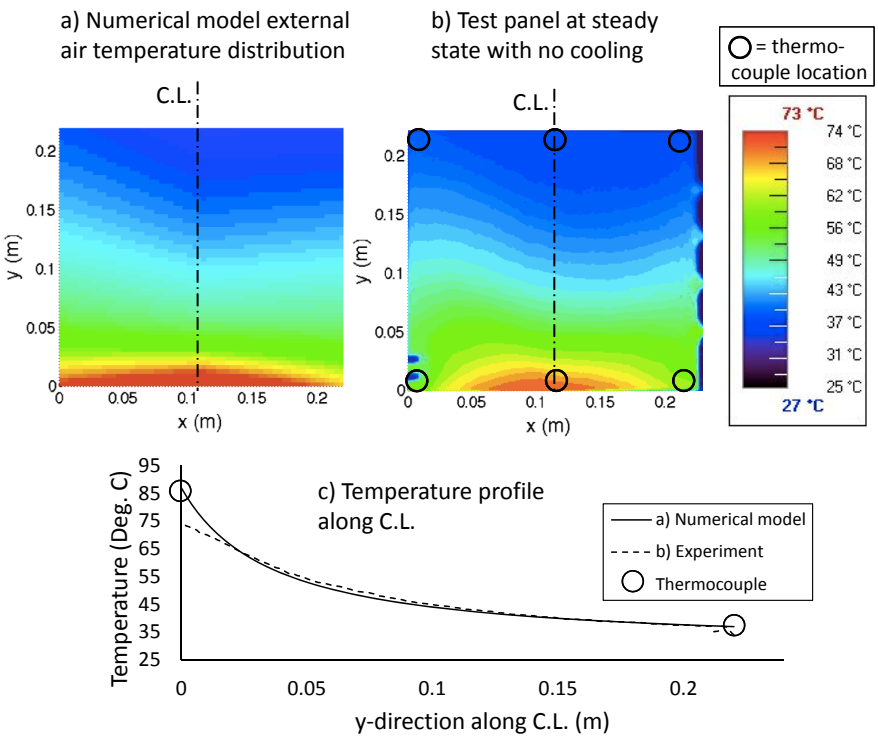

Figure 4: Surrounding air temperature baseline calibration.

the two experiments suggest that it may be used as a reliable proxy for the thermodynamics of the physical system in similar panel designs.

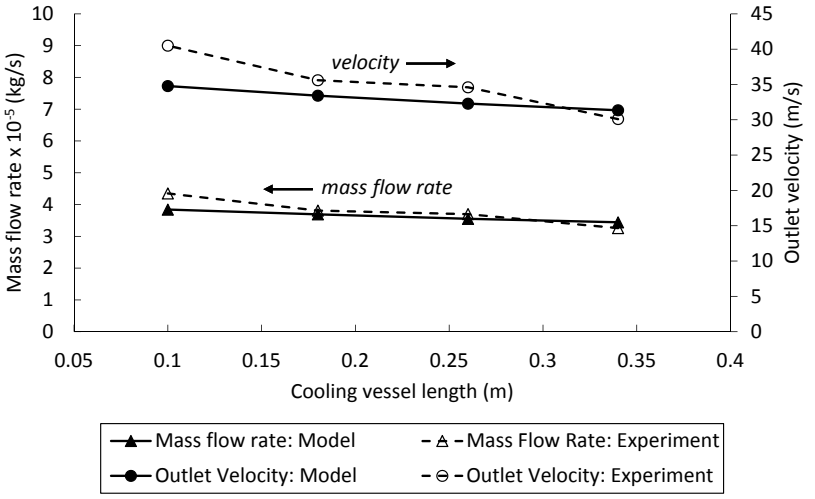

Figure 5: Summary of mass flow rate and outlet velocity using calibrated inlet pressure of 1.2 bar.

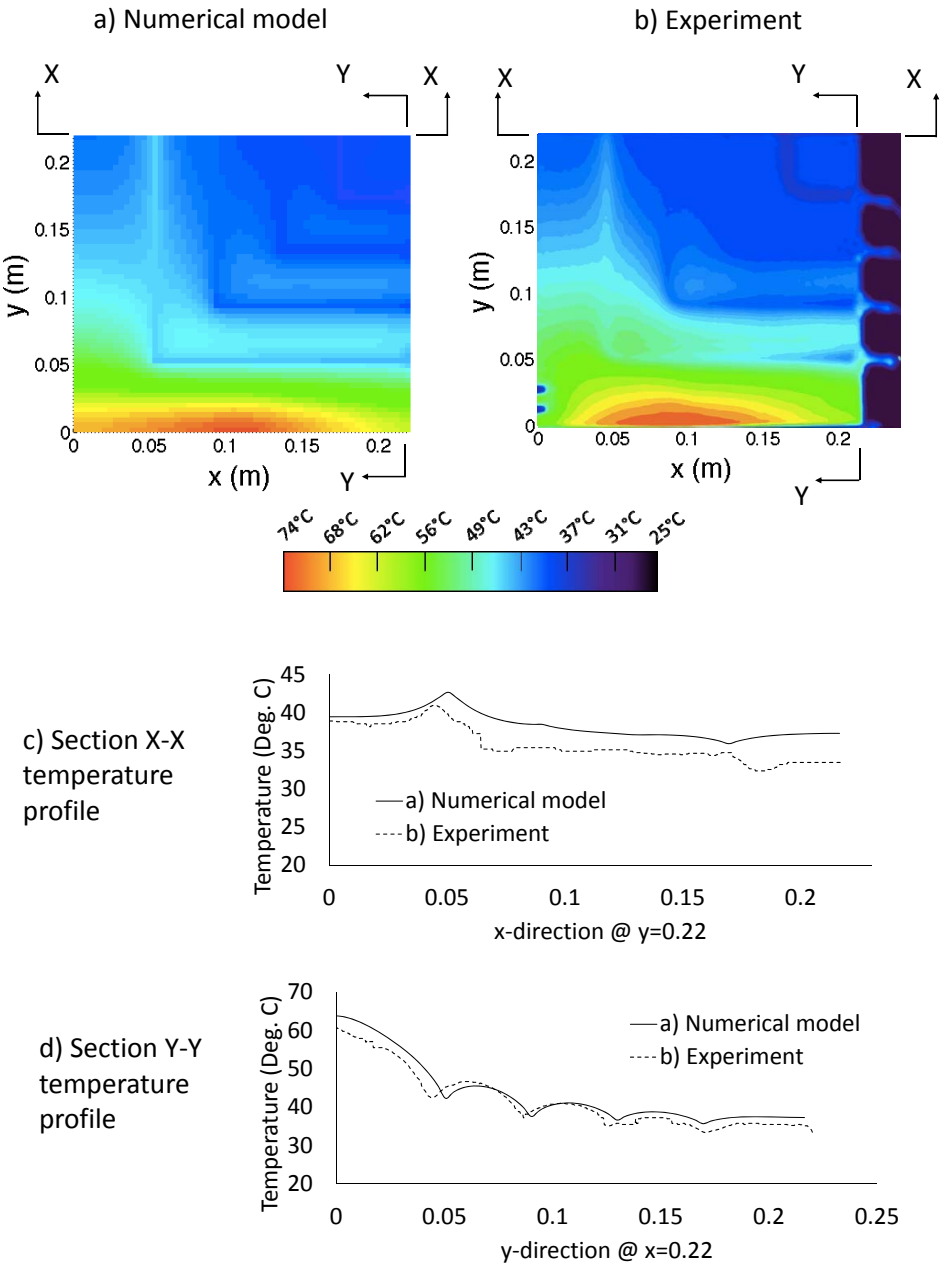

Figure 6: Numerical and experimental data correlation for: $P_{in} = 1.08$ bar, $T_{in,1-4} = [43\ 38\ 37\ 36]$°C.

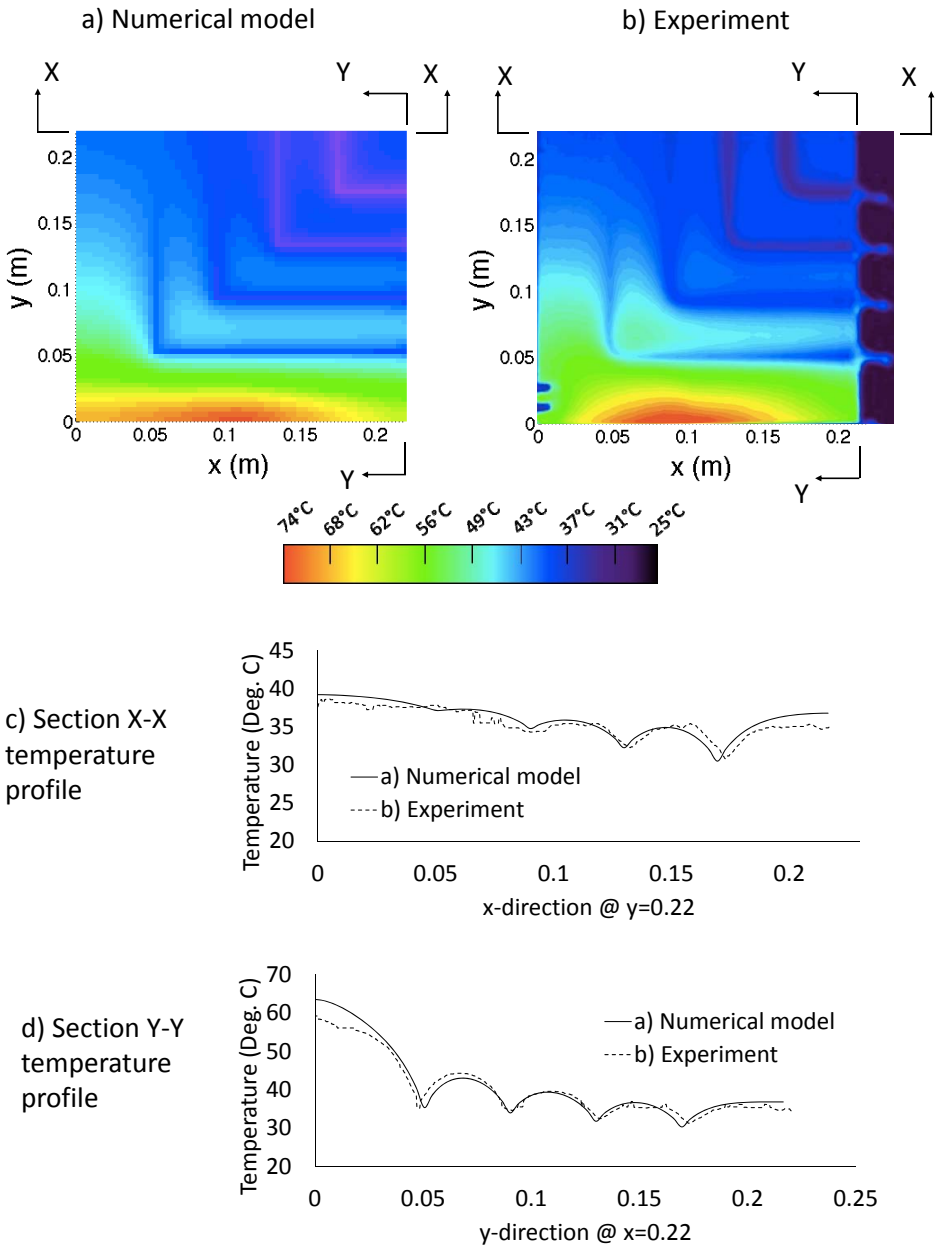

Figure 7: Numerical and experimental data correlation for: P_{in} = 1.2 bar, $T_{in,1-4}$= [38 36 33 31]°C.

5. Optimisation

An automatic optimisation procedure is demonstrated in this section to identify suitable performance metrics and establish a thermal design methodology for vasculature topology in a thin panel. The design methodology can be extended to the general case of a gas turbine compressor blade. Design of vascule topology for a combined film-heat exchange cooling system, as described in Section 1, is complex due to the fact that, a heat transfer loop is formed between the internal coolant flow and the external film flow. The methodology presented here results in designs where this is taken into account and each cooling mode is utilized without undermining the performance of the other.

In this study, focus is on the thermal behaviour of a 0.1 m x 0.1 m panel containing a single internal vessel. A modelling assumption is made of transverse vasculature homogeneity in a wide span panel and thus the treatment of thermal boundary layer growth in the single vessel model can reasonably be reduced in the freestream direction only. While in any industrial application one would anticipate several such vessels being embedded in the composite material, modelling this more complex scenario is a relatively straightforward extension of the proof-of-concept shown here. To reflect the geometry of a typical heat exchanger and to enforce reasonable constraints on inlet and outlet positions, the vessel is defined to take the form of the real part of a complex sinusoid. The design parameter vector [A B C D] is defined according to the function

$$y = Ae^{x}sin(Bx)(1/480) + (1/A)e^{-x}sin(Cx) + sin(Dx) \tag{12}$$

where y is the spanwise ordinate, x increases in the direction of the gas stream, and (1/480) in the first term is an empirically determined scaling constant. The sinosoid was chosen and defined as shown in equation (12) in an attempt to minimize the number of design parameters but maximize the number of possible vascule topology configurations. Figure 8 illustrates several distinct vessel topology configurations that can be obtained by varying the four design parameters in equation (12). Fabrication techniques and/or constraints were not considered in the optimisation study, however, imposing a minimum radius constraint on the sinosoid function may be an effective means to enable fabrication using the same technique described in Section 3. In each of the sample panels shown in Figure 8 , the cool film originates along the edge of the panel at $x = 0$.

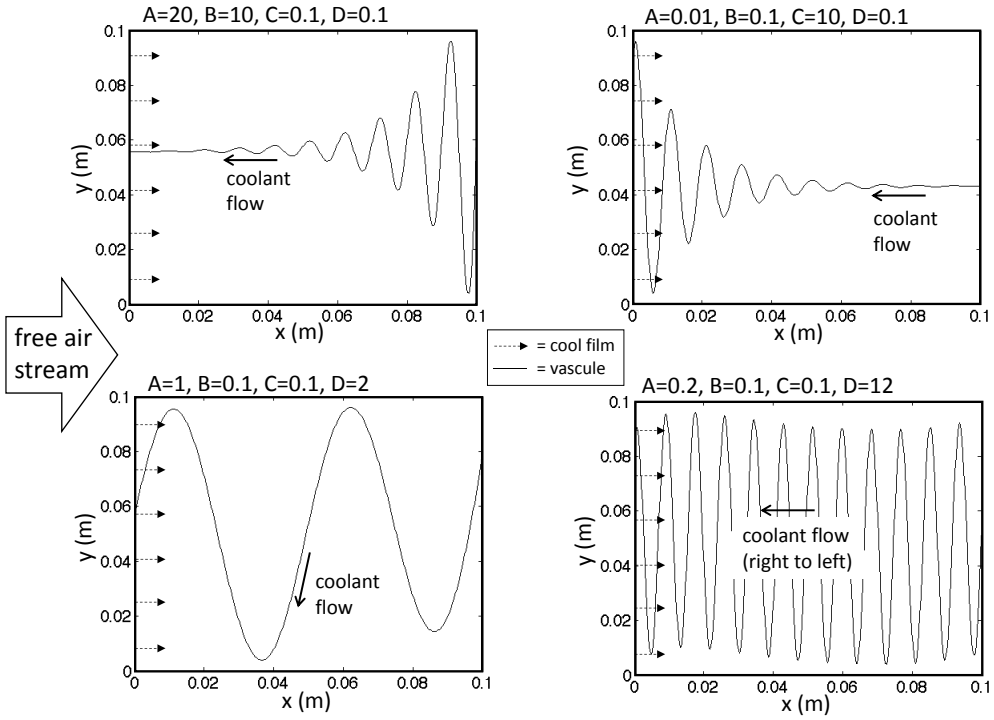

Figure 8: Possible vessel topology using (12). Cool films originate along thge entire panel edge coincident with the y-axis.

Reliability of the methodology is dependent on robustness of performance over a range of metrics. The simplest objective is to seek the lowest maximum temperature, since structural integrity is constrained by the proximity to the material T_g at the most susceptible location. However, simply minimizing the maximum panel temperature may not be a suitable basis for optimal design since other regions of the panel might receive more cooling than necessary to remain below T_g, and one could anticipate incurring an unnecessary penalty in structural efficiency. One can account for the distribution of the structural penalty without feeding back additional objectives (which would greatly restrict the choice of optimisation strategies) by instead considering average temperature across the panel. However, once again this optimisation objective may be vulnerable to suboptimal or invalid designs returning an attractive performance value. A low average value would not necessarily satisfy the independent constraint that temperatures should everywhere remain below the material T_g. It would seem necessary, at least a priori, to invoke

second order statistical quantities to constrain the metric sufficiently well to deliver practical and efficient designs. Three panel temperature performance metrics were considered in the optimisation study namely maximum, average, and standard deviation. The standard deviation of panel temperature is defined by

$$T_{dev} = \sqrt{\frac{1}{n-1}\sum_{i=1}^{n}(T_i - \bar{T})^2} \tag{13}$$

where n is the number of points discretising the panel and $\bar{T}$ is the mean temperature.

The local performance space was evaluated on the 0.1 m x 0.1 m panel using a perturbation technique to estimate gradients and Newton's method of steepest descent to determine the choice of step size in the parameter space. A refined implementation of this method, known as a dynamic hill-climber [23] was performed using a Rolls Royce proprietary optimisation software package [24] which executes the numerical model described in Section 2 at each iteration. Freestream air temperature, freestream air velocity, coolant inlet temperature, coolant inlet pressure, and vascule section radius were kept constant and defined as 100°C, 400 m/s, 25°C, 1.2 atm, and 0.5 mm respectively. These conditions are meant to be somewhat representative of a compressor blade environment within a gas-turbine engine, however, for the purpose of this study their exact values are not critical. Approximately 500 numerical iterations were performed for each case.

Figures 9, 10, and 11 illustrate the convergence for the range of performance metrics introduced above: minimising the temperature extremum, minimising the average, and minimising the standard deviation, while keeping constant the temperature and mass flux of the coolant and gas stream. The optimiser rapidly finds local minima, but in common with all such gradient-based schemes, there is no guarantee of reaching a global extremum. Thus once converged, the dynamic hill-climber adds several random perturbations to the parameter vector in the hope that it will re-converge to the same optimal vector, building confidence in the robustness of this particular local minimum, or alternatively escape the current local extremum and find an even better solution. Each suitably re-converged minimum vascule geometry and predicted panel temperature distribution is shown to a resolution of 1.66 mm. In Figures 9 - 11, the external gas stream flows from left to right,

and the coolant exits over the leading edge in cases where film cooling is included (see Figure 8). The best design obtained is illustrated by a thicker border on the inset image.

It is clear from comparing local minima in Figure 9a that large amplitude oscillations of the vessel pathway are somewhat better at reducing the maximum temperature, simply because heat is more effectively removed from all regions of the panel. With film cooling considered in the model, the plots in Figure 9b of local minima appear to offer a broader range of useful configurations. All are naturally characterised by a reduced need for internal cooling towards the (left) leading edge of the panel, since external cooling is most effective here, though the helpful influence decays exponentially towards the trailing edge as hot gas stream mixes progressively into the boundary layer and dilutes the coolant emission.

When the performance metric is changed to an average temperature condition, as shown in Figure 10a, the tendency to favour large amplitude oscillations is more pronounced. In order for the thermal footprint of the vessel to cover the full span of the panel, the half-power width of the near-Gaussian temperature distribution around the vessel must extend to reach the panel boundary. Thus, the amplitude is governed jointly by the thermal diffusion coefficient and the local temperature difference. Similarly, the optimal oscillation frequency scales with the half-power width, though it should be noted that for a given target average temperature, the optimal frequency varies in the streamwise direction as the coolant flow progressively warms. Although not from the global optimal design, a tendency towards this frequency variation in the final local minimum in Figure 10a can be seen. With film cooling, not only is a lower average temperature obtained in a like-for-like comparison of optimal geometries without film cooling, but the frequency of the vessel topology is substantially lower, indicating a potential reduction in any structural penalty associated with inclusion of the cooling vessels.

Considering the second order statistical moments of the temperature is arguably the most suitable performance metric, since one would expect the temperature variance to be more closely tied to the quality and 'design efficiency' of the vessel topology and less strongly correlated with the particular boundary conditions used in this example. Figure 11a shows the optimal topology without film cooling and Figure 11b shows the effect of film cooling. Unlike earlier metrics, here it is appropriate to make a quantitative comparison of the variance values. The panel with film cooling has a temperature variance 18% smaller than the case without film cooling.

One risk in using an automatic system for optimisation may be that a geometry that best satisfies the target criterion may have circumvented other (perhaps practical) constraints on the design that are not captured by the automated process. For example, the considerations of structural performance degradation caused by the presence of the vasculature have not been incorporated into the automatic process. One approach to gage relative structural robustness is based on total cooling vessel length using the reasoning that if total cooling vessel length is minimized, adverse effects on the structure are also minimized. Figure 12 compares geometry from cases with and without cool films. In all cases, an increase in performance and a reduction in vessel length ranging between 7% and 28% is seen if a cool film is included. This finding indicates that use of a cool film may improve structural efficiency for a vascularized panel.

Similarly, another concern, is that optimisation of one metric may have an adverse effect on another. To mitigate that risk, the relative consequences of one performance metric over another are examined. As shown in Figure 13 on a normalised scale, there is a strong correlation between optimality in all three metrics, though naturally there is significantly wider range of variances en route to convergence than for maximal and average metrics. This offers some reassurance that design performance is robust to the choice of metric.

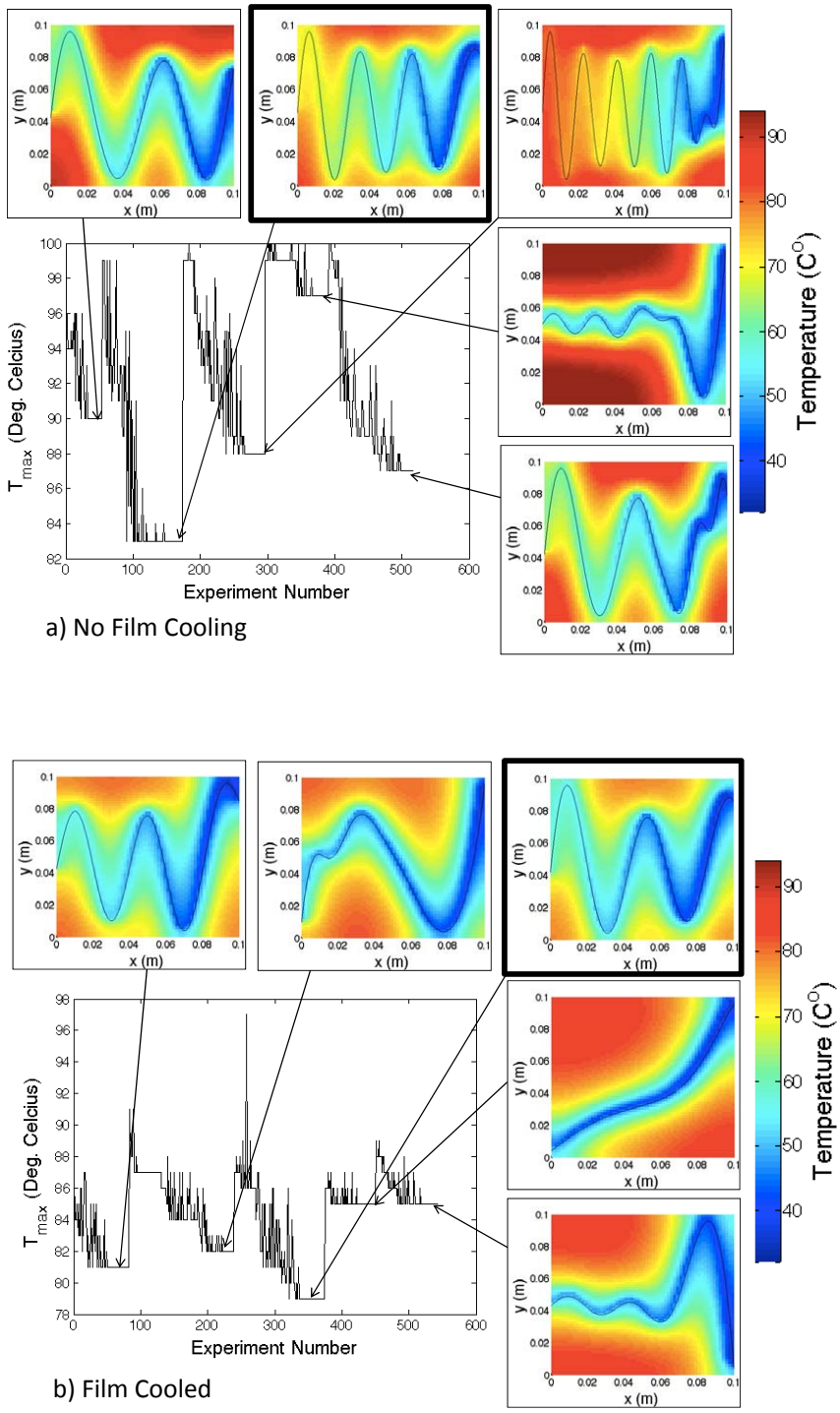

Figure 9: T_{max} optimisation.

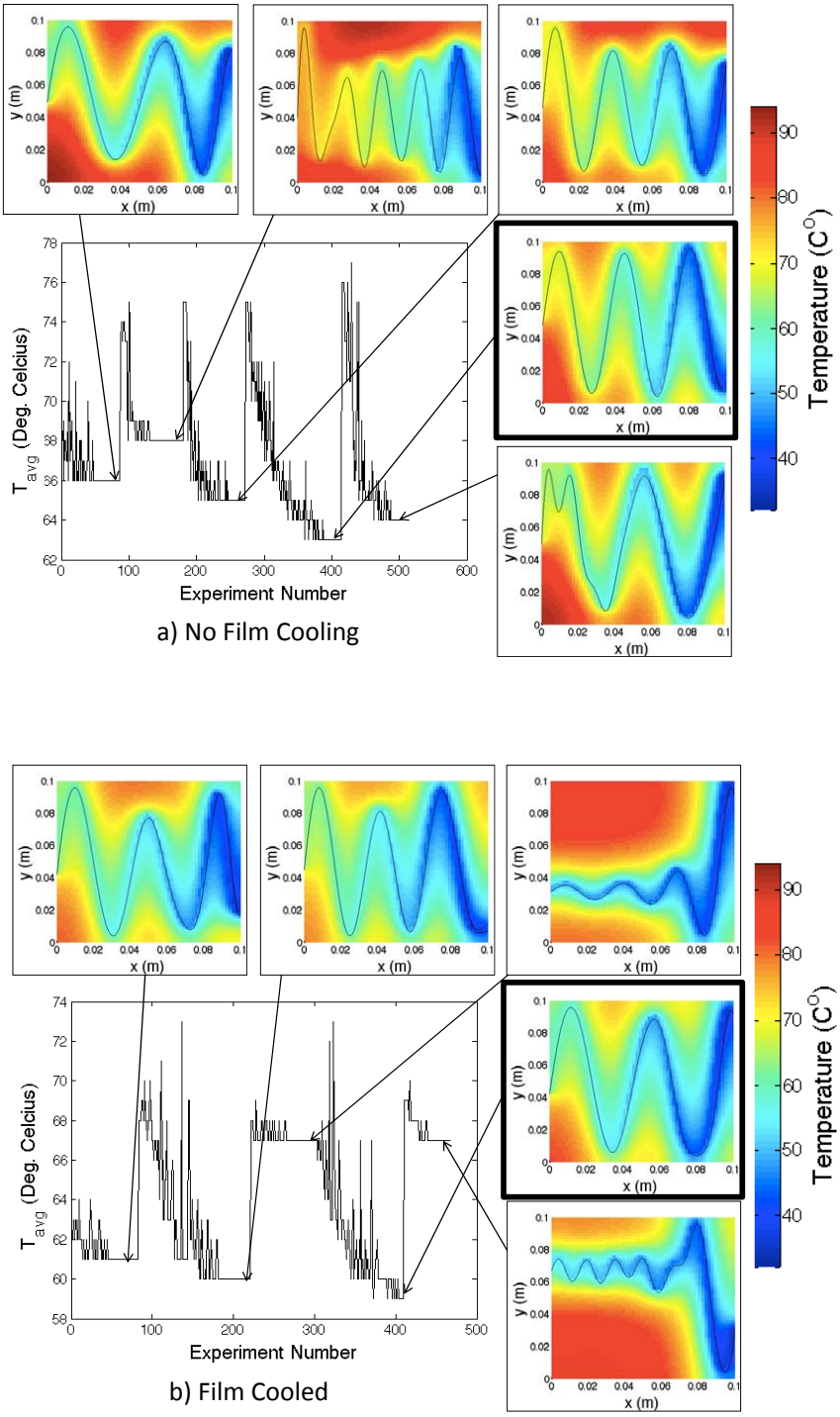

Figure 10: T_{avg} optimisation.

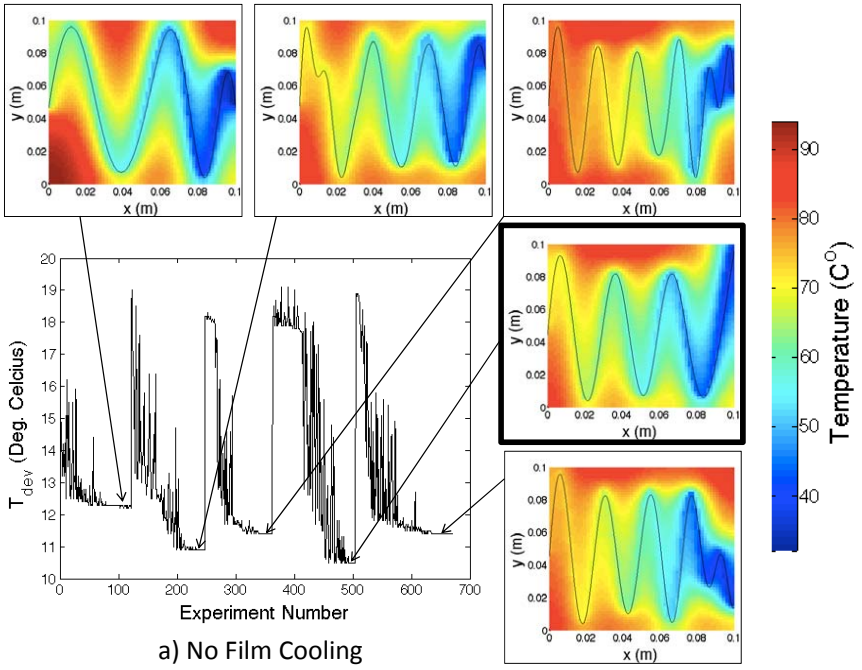

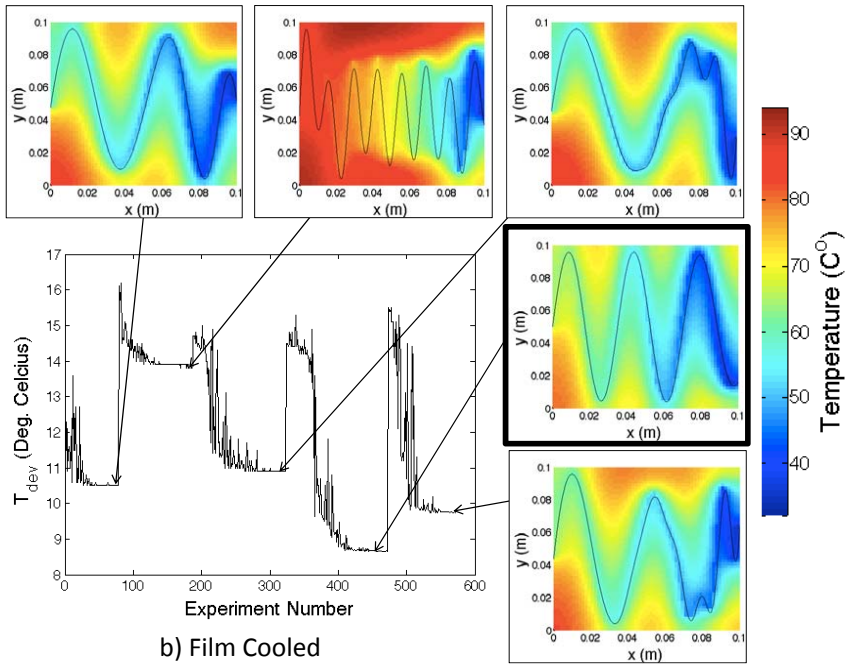

Figure 11: T_{dev} optimisation.

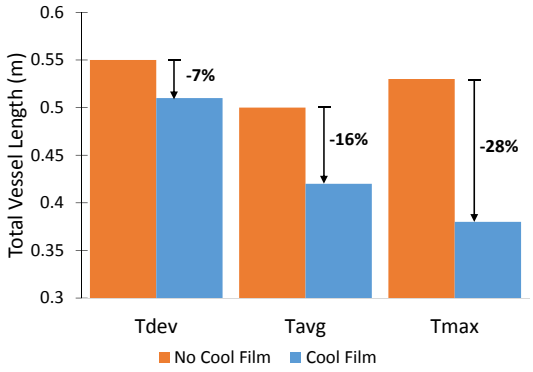

Figure 12: Total vessel length with and without film cooling.

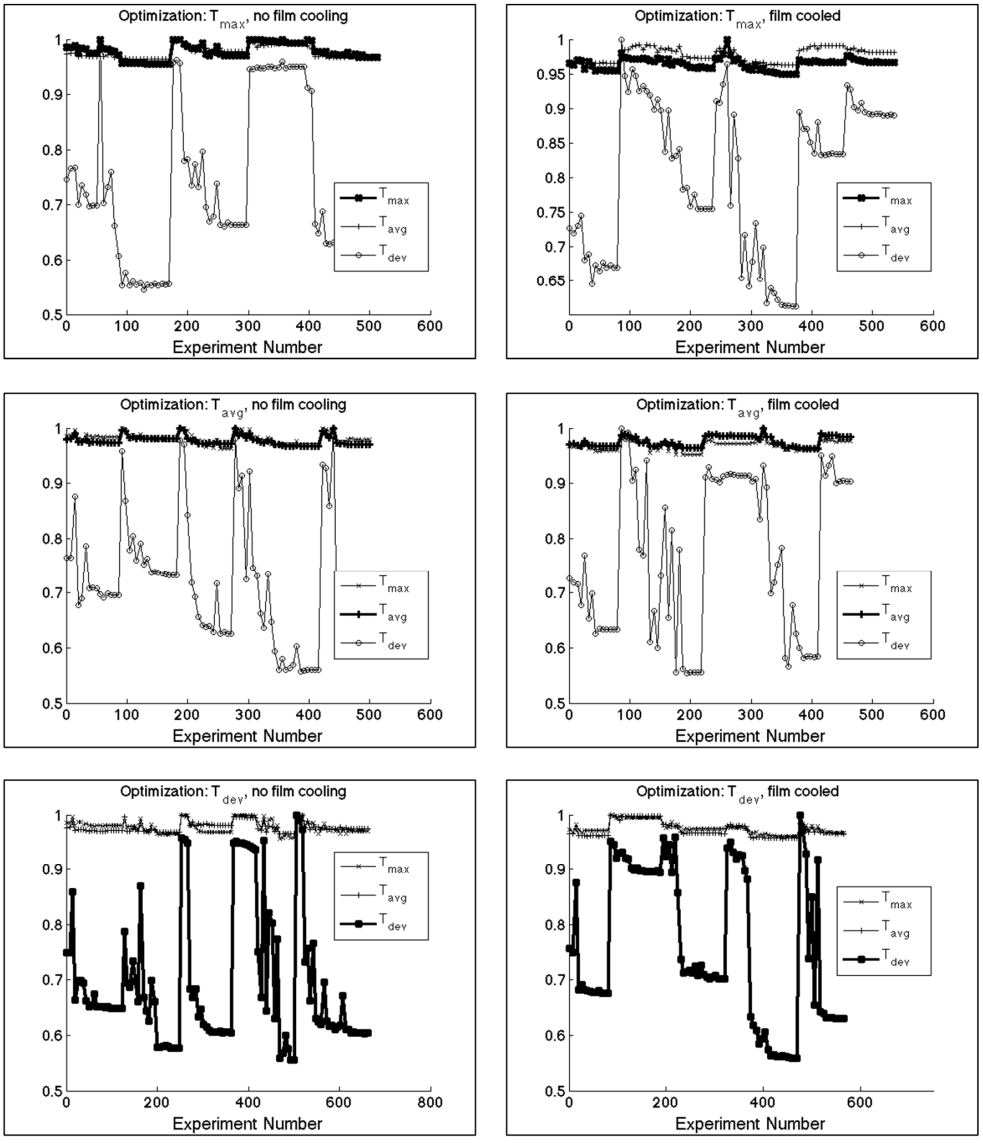

Figure 13: Optimization metric commonality

6. Conclusion

An investigation was conducted on the use of CFRP composite materials for structural components in gas turbine engines. Use of polymer materials in elevated temperature environments, such as a gas turbine engine, requires an active cooling strategy to ensure they remain below their glass transition temperature. An experimentally validated numerical model was created that is capable of a thermal simulation of a thin composite panel actively cooled by an internal vascular network and an external boundary layer film. An optimisation study was then conducted using the numerical model to study the effect of external film cooling on an efficient internal vasculature topology design. An improvement in performance is observed if film cooling is included, as measured by maximum, average, and deviatory panel temperatures. The improved performance is accompanied by a reduced internal vasculature length. In performing the optimisation study, an effective thermal design methodology was demonstrated for an actively cooled thin composite plate. The numerical model, optimisation findings, and overall design methodology are trivially extensible to a structure with more complex geometry and vasculature topology such as a cooled composite compressor blade in a gas turbine engine.

7. Acknowledgments

This work was funded by The University of Bristol. The authors thank Dr. Shahrokh Shahpar (Rolls Royce 3D Geometry, Meshing, and Optimization, Rolls Royce plc., Derby, UK) and Rolls-Royce for allowing us the use of their proprietary optimisation software package, SOFT [24].

8. References

[1] A. Copolla, N. Sottos, S. White, Active cooling of vascularized composites for application at elevated temperatures, in: American Society for Composites 29th Technical Conference/16th US-Japan Conference on Composite Materials, La Jolla, CA, 2014.

[2] SE 70 low temperature cure high toughness epoxy prepreg system, datasheet level 1, PDS-SE70-0314, http://www.gurit.com (2014).

[3] Hexply 8552 epoxy matrix (180C/356F curing matrix) product data, FTA 072e, http://www.hexcel.com (2013).

[4] G. Smith, Gas Turbines and Jet Propulsion for Aircraft, 4th Ed., Aircraft Books Inc., 1946.

[5] E. Eckert, Transpiration and film cooling, Heat-Transfer Symposium (1952) 195–210.

[6] R. Goldstein, E. Eckert, V. Eriksen, J. Ramsey, Summary report film cooling following injection through inclined circular tubes, NASA CR-72612, 1969.

[7] I. Treager, Aircraft and Gas Turbine Engine Technology, 3rd Ed, Glencoe/McGraw-Hill, 1995.

[8] J. Mattingly, Elements of Gas Turbine Propulsion, McGraw-Hill, Inc., 1996.

[9] M. Lyall, A. Williams, B. Arrit, B. Taft, Experimental analysis of a biologically inspired thermal-structural satellite panel, 49th AIAA/ASME/ASCE/AHS/ASC Structures, Structural Dynamics, and Materials Conference, 7-10 April, Schaumburg, IL.

[10] A. Williams, R. Underwood, B. Arritt, G. Busch, B. Taft, Biologically inspired multifunctional composite panel with integrated thermal control, in: 51st AIAA/ASME/ASCE/AHS/ASC Structures, Structural Dynamics, and Materials Conference, Orlando, FL, 2010.

[11] B. Kozola, V. Shipton, K. Christensen, Characterization of active cooling and flow distribution in microvascular polymer, Journal of Intelligent Material Systems and Structures 0 (2010) 1–10.

[12] M. Pierce, Microvascular heat transfer analysis in carbon fiber composite materials, Master's thesis, University of Dayton, Ohio (August 2010).

[13] D. Phillips, M. Pierce, J. Baur, Mechanical and Thermal Analysis of Microvascular Networks in Structural Composite Panels, Composites Part A 42 (2011) 1609–1619.

[14] S. Soghrati, A. Najafi, J. Lin, K. Hughes, S. White, N. Sottos, P. Geubelle, Computational analysis of actively-cooled 3D woven microvascular composites using a stabilized interface-enriched generalized finite element method, International Journal of Heat and Mass Transfer 65 (2013) 153–164.

[15] J. Lee, S. Lorente, A. Bejan, Vascular design for thermal management of heated structures, The Aeronautical Journal 113(1144) (2009) 397–407.

[16] J. Lee, S. Lorente, A. Bejan, Transient cooling response of smart vascular materials for self-cooling, Journal of Applied Physics 105(6) (2009) 064904.

[17] L. Rocha, S. Lorente, A. Bejan, Tree-shaped vascular wall designs for localized intense cooling, International Journal of Heat and Mass Transfer 52 (2009) 4535–4544.

[18] K. Wang, S. Lorente, A. Bejan, The transient response of vascular composites cooled with grids and radial channels, International Journal of Heat and Mass Transfer 52 (2009) 4175–4183.

[19] H. Blasius, Grenzschichten in Flussigkeiten mit kleiner Reibung, Z. Math Physik 56 (1908) 1–37.

[20] B. Cushman-Roisin, Environmental Fluid Mechanics, John Wiley and Sons, 2014.

[21] C.-Y. Huang, R. Trask, I. Bond, Characterization and analysis of carbon fibre-reinforced polymer composite laminates with embedded circular vasculature, Journal of The Royal Society Interface 7 (49) (2010) 1229–1241.

[22] CES EduPack software, Granta Design Limited, Cambridge, UK, http://www.grantadesign.com (2009).

[23] D. Yuret, M. De La Maza, Dynamic hill climbing: Overcoming the limitations of optimization techniques, in: The Second Turkish Symposium on Artificial Intelligence and Neural Networks, Citeseer, 1993, pp. 208–212.

[24] S. Shahpar, SOFT, Rolls-Royce, Derby, UK, 2013.